Journal of Energetic Materials
Publication details, including instructions for authors and subscription information:
http://www.informaworld.com/smpp/title~content=t713770432

Molten salt destruction of energetic materials: Emission and absorption measurements

Michelle L. Pantoya[a]; Benjamin D. Shaw[b]
[a] Mechanical Engineering Department, Texas Tech University, Lubbock [b] Mechanical and Aeronautical Engineering Department, University of California, Davis

To cite this Article Pantoya, Michelle L. and Shaw, Benjamin D.(2002) 'Molten salt destruction of energetic materials: Emission and absorption measurements', Journal of Energetic Materials, 20: 1, 1 — 37
To link to this Article: DOI: 10.1080/07370650208244812
URL: http://dx.doi.org/10.1080/07370650208244812

MOLTEN SALT DESTRUCTION OF ENERGETIC MATERIALS: EMISSION AND ABSORPTION MEASUREMENTS

Michelle L. Pantoya
Mechanical Engineering Department
Texas Tech University, Lubbock

Benjamin D. Shaw
Mechanical and Aeronautical Engineering Department
University of California, Davis

ABSTRACT

Spectroscopic aspects of decomposition behaviors of the high explosives LX-17 (92.5 wt % 1,3,5-triamino-2,4,6-trinitrobenzene (TATB) plus 7.5 wt % Kel-F 800 plastic binder), LX-04 (85 wt % octahydro-1,3,5,7-tetranitro-1,3,5,7-tetrazocine (HMX) plus 15 wt % Viton A plastic binder), and 2,6-Dinitrotoluene (DNT) were investigated when 0.3 or 1.0 g samples were immersed into molten salt baths (700 °C molten LiCl-NaCl-KCl eutectics). UV-VIS absorption measurements provided an indication of intermediate chemical species present in the salt baths during sample decomposition, and measurements of emission spectra allowed temperatures of soot within reacting DNT gas bubbles to be inferred. The soot temperatures were close to calculated values of adiabatic flame temperatures. In addition to advancing fundamental knowledge, these results are of use for aiding in the design of molten-salt reactors.

Journal of Energetic Materials Vol. 20, 001-037 (2002)
Published in 2002 by Dowden, Brodman & Devine, Inc.

INTRODUCTION

As a result of the end of the Cold War and the shift in emphasis to a smaller stockpile, many munitions, both conventional and nuclear, are scheduled for dismantlement. Major components of these munitions are energetic materials. Although recycling and reuse are the preferred methods for dealing with these surplus materials, it will always be necessary to destroy intractable or unusable energetic materials. Open detonation and open burning have been used as methods of destruction. However, these methods can produce pollutants that are released directly into the atmosphere. Another method that has received attention is the molten salt destruction (MSD) process.[1] In this process, energetic materials are injected into hot molten salt baths, where they decompose. Researchers at the University of California, Davis and the Lawrence Livermore National Laboratory are studying the molten salt destruction process as an attractive means of destroying energetic materials in an environmentally benign fashion. This article presents research on fundamental behaviors of energetic materials immersed into molten salt baths.

In this research, decomposition behaviors of the high explosives LX-17 (92.5 wt % 1,3,5-triamino-2,4,6-trinitrobenzene (TATB) plus 7.5 wt % Kel-F 800 plastic binder), LX-04 (85 wt % octahydro-1,3,5,7-tetranitro-1,3,5,7-tetrazocine (HMX) plus 15 wt % Viton A plastic binder), and 2,6-dinitrotoluene (DNT) were investigated when samples initially between 0.3 and 1.0 g were

immersed into molten salt baths (700 °C molten LiCl-NaCl-KCl eutectics). UV-VIS absorption measurements provided an indication of intermediate chemical species during sample decomposition. Using emission measurements, temperatures of soot within reacting gas bubbles were also estimated.

In the following text, the apparatus used for the experiments is described first. Following this, results of the measurements are presented, and conclusions are then drawn.

EXPERIMENTAL DESCRIPTION

The apparatus used in the spectroscopy experiments is illustrated schematically in Fig. 1. This apparatus is similar in some respects to a molten salt spectroscopy system described elsewhere,[2] though significant differences exist between the systems. All of the spectroscopy experiments were performed in a specially designed high-temperature furnace. Two view ports were located on opposite sides of the furnace. A fiber optic cable connected to a coupling lens was fastened into each view port. The input and output of each fiber optic cable had a 50-μm diameter. A deuterium light source provided a high-output high-stability fiber optic light source optimized for the UV. This deuterium lamp produced intense, continuous spectral output from about 200-400 nm, making it especially useful for measurements in the UV. In addition, a xenon flash lamp also provided a broadband light source for the range 250-700 nm.

One cable brings light from the deuterium or xenon light source into the furnace. After exiting the optical fiber and coupling lens, the beam is collimated with a diameter of about 5 mm and directed through the furnace. The beam passes through a 20 × 20 mm cross-section quartz cell (cuvette) that contains the molten salts. The beam is then received by a coupling lens and fiber optic cable positioned directly behind the quartz cell and aligned with the first view port. This receiving cable is connected to an Ocean Optics SD 1000 Fiber Optic Spectrometer that interfaces with a Pentium 5-90 PC. In the spectrometer, light from the optical fiber impinges on a concave front-silvered mirror with a holographically inscribed diffraction grating. The diffracted spectrum is directed to a silicon charge-coupled diode array. With "OOIBase" software provided by Ocean Optics Inc., absorption and emission spectra were measured. This software allows time-series data acquisition. Using this capability, intermediate (transient) chemical species present in the salt bath were evaluated. This same system was also used to detect radiant emissions from the samples. This was accomplished with the deuterium or xenon flash lamp turned off.

The spectrometer was calibrated for absorbance measurements using a mercury-argon calibration source for the UV-VIS-NIR spectral wavelength region. The spectral lines produced by the mercury-argon calibration source are in the range 253.65-922.45 nm. For emission measurements, the spectrometer was calibrated against a tungsten halogen light source with a 3100 K color

temperature. The calibration data for this source include absolute intensities for wavelengths in the range 300-1000 nm.

The 1.0 g DNT samples were melt-cast onto the tips of 3 mm-diameter quartz rods, and the 0.3 g LX-04 and LX-17 pellets were adhered to the tip of similar quartz rods using high-temperature adhesive. The quartz rods were connected to an air-piston cylinder via a stainless steel drill chuck; the samples were injected into the chloride molten salts via the air-piston cylinder.

Two beam locations in the molten salt relative to the sample position were studied. The upper location is illustrated in Fig. 2, where the nearest beam edge was positioned approximately 2 mm above the decomposing sample (beam location 1 in Fig. 2). This beam position allows detection of chemical species above the sample. It is noted that the quartz rod that held the sample in position did not influence the spectroscopic results. This was verified by repeated experimentation with known species (i.e., acetone and toluene) with and without interference of the quartz rod. Repositioning the quartz rod relative to the beam and obtaining consistent and repeatable results from energetic materials decomposing in the molten salt also verified this.

In the second arrangement, i.e., beam location 2 in Fig. 2, the nearest beam edge was positioned approximately 2 mm below the decomposing sample and directly above the base of the quartz

cuvette. This beam location allowed investigation of regions beneath the samples. Residence times should be different for species detected above the samples relative to species detected below the samples, which could lead to different species being present at the locations investigated. This hypothesis was verified in the experiments, as described later.

Visualization experiments, details of which are described elsewhere,[3,4] were conducted in a larger furnace with quartz containers holding the molten chloride salts. These containers held 300 cc of molten salt. The visualization experiments employed essentially the same sample injection system that was used in the spectroscopic experiments, with one exception. The LX-17 and LX-04 samples were mounted on stainless steel rods with the same dimensions as the quartz rods used in this study. A borescope was used to view a sample once it was injected into the molten salts. A borescope is a visual inspection device that uses fiber optics to provide optical access to remote areas. The borescope and cooling assembly[5] were mounted in the furnace and positioned directly outside the transparent beaker of molten salts. A Kodak EktaPro 1000 high-speed motion analyzer was connected to the borescope. Using a stainless steel rod in place of a sample, the camera was focused and aligned. Once the camera was focused, the sample was immediately injected into the salts. The motion analyzer captured images at 1000 frames per s (fps). In order to provide sufficient light to record at these frame rates, a 1000 W halogen lamp was used as a backlight. This light

was placed in the molten salts, and a quartz tube prevented the light bulb from coming into direct contact with the molten salts. After images were recorded, a video copy processor was used to produce individual single-frame images for detailed analysis.

RESULTS AND DISCUSSION

Emission Measurements

In order to better interpret emission spectra collected from decomposing samples, the overall decomposition behaviors of LX-17, LX-04 and DNT, as observed from the photographic images, will be summarized first. Figure 3 is a schematic diagram comparing the behaviors observed during LX-17, LX-04 and DNT decomposition in the molten salts. Both LX-17 and LX-04 behaved similarly. In each case, liquid salts came into direct contact with sample surfaces, and bubbles formed and expanded on the sample surfaces. When bubbles left the LX-17 and LX-04 samples they were mature, i.e., they maintained a constant size and color, and they were always fairly transparent. During the decomposition of DNT however, markedly different behaviors were observed. For DNT decomposition, there was always a thin vapor film that separated the salt from the sample. As vapor in the film left the top of a sample, bubbles formed, pinched off, suddenly increased in size and darkened in color, and moved along the quartz rod until they were out of the field of view.

The rapid growth and darkening of the DNT bubbles indicated that the chemical species that left the DNT samples were reactive and that chemical reactions occurred in the bubbles after they left the samples.[3] The DNT bubble volumes increased by about a factor of 70, indicating that heat transfer from the salts did not dominate bubble size changes. A chemical equilibrium code[6] predicts that a primary decomposition product of DNT is solid-phase carbon; hence, the darkening in DNT bubbles may be soot produced during chemical reactions that occur in the bubbles.

As LX-17 and LX-04 decomposed, no emitted light was detected in the spectrum investigated (200-1000 nm). The gas bubbles generated during LX-17 and LX-04 decomposition did not expand or change size, and they were relatively transparent, indicating that the amount of soot produced in the bubbles was minimal. The gas species inside the bubbles would have radiated light. However, the intensity of this radiation was weak and not detectable in these experiments.

During DNT decomposition, however, broadband emissions were detected starting at about 450 nm and increasing in intensity until about 600 nm, after which detector roll-off occurred. Figure 4 shows representative emission spectra for DNT (note that the vertical axis is actually $\log_{10}$ of the emission measurement). These emissions likely result from soot that is apparently produced in the DNT bubbles. Calculations of the adiabatic flame temperature for DNT indicate that any soot present would emit

light vigorously in the visible spectrum. From the DNT emission spectra in Fig. 4, the temperature of radiating soot particles can be estimated using two-wavelength pyrometry. These temperature estimates are a good indication of gas temperatures within the bubbles, assuming the gas and soot temperatures are in equilibrium.

In two-wavelength pyrometry temperature is obtained from the ratio of light intensity emitted at two different wavelengths. The analysis uses the definition of spectral emissivity.[7]

$$\varepsilon_\lambda = \frac{I_\lambda}{I_{\lambda b}} \tag{1}$$

In Eq. (1), I_λ and ε_λ are the emission intensity and spectral emissivity at wavelength λ, respectively, and $I_{\lambda b}$ is the emission intensity of a black body. It has been shown[8] that the spectral emissivity of soot may be approximated as shown in Eq. (2),

$$\varepsilon_\lambda = 1 - e^{\frac{-7fL}{\lambda}} \tag{2}$$

where f is the soot volume fraction and L is the optical path length. The soot volume fraction is the ratio of the volume of soot to the total volume of decomposition products (Eq. (3)).

$$f = \frac{m_{soot}}{m_{total}} \frac{\rho_{total}}{\rho_{soot}} \tag{3}$$

In Eq. (3), ρ is the density of soot or the total density of decomposition products, and m represents the mass of soot or the total mass of decomposition products. The product of the soot volume fraction and optical path length may vary for each bubble. Therefore, limits were placed on possible values for the ratio $7fL/\lambda$. Specifically, three cases were analyzed: when $7fL/\lambda$ is significantly greater than one, approximately equal to one, and significantly less than one. These limits provide an approximate temperature range for radiating soot particles and gases within the bubbles. Using a chemical equilibrium code[6] and available data on the density of solid carbon, the soot volume fraction in bubbles composed of equilibrium DNT decomposition products is estimated to be about 1×10^{-5}. For the wavelength range 200-600 nm and a representative optical path length of 1 cm, the ratio $7fL/\lambda$ varied from 1.2 to 3.5 for $f = 10^{-5}$.

The emission intensity at the wavelength λ_1 can be expressed as a function of the temperature T, an instrument-related calibration correction factor k, and the black body radiation constants C_1 and C_2 (see Eq. (4)).

$$I_{\lambda 1} = kC_1\left(1 - e^{\frac{-7fL}{\lambda_1}}\right)\left[\lambda_1^5\left(e^{\frac{C_2}{\lambda_1 T}} - 1\right)\right]^{-1} \qquad (4)$$

Ratios of Eq. (4) can be applied to any two wavelengths using the corresponding emission measurements shown in Fig. 4. In applying

Eq. (4), it is noted that $e^{C_2/T\lambda_1} >> 1$ typically holds. As a result, the approximation $e^{C_2/T\lambda_1} - 1 \approx e^{C_2/T\lambda_1}$ was used here. The wavelength ratio will vary according to the limit placed on $7fL/\lambda$. In the limit where $7fL/\lambda$ is significantly less than unity, the spectral emissivity can be expanded in a Taylor series, with only the largest term retained.

$$\varepsilon_\lambda = 1 - \left(1 - \frac{7fL}{\lambda} + \ldots\right) \approx \frac{7fL}{\lambda} \tag{5}$$

Upon neglecting higher order terms, the spectral emissivity reduces to the ratio $7fL/\lambda$. For the upper limit, when $7fL/\lambda$ is appreciably greater than unity, the emissivity approaches a value of unity. By using a ratio of emission measurements at two wavelengths, the temperature can then be determined for each limiting case according to the following equations.

$$\begin{aligned}
&\frac{7fL}{\lambda} << 1 && \frac{I_{\lambda_1}}{I_{\lambda_2}} = \frac{\lambda_2^6}{\lambda_1^6} \frac{e^{\frac{C_2}{T\lambda_2}}}{e^{\frac{C_2}{T\lambda_1}}} \\
&\frac{7fL}{\lambda} \approx 1 && \frac{I_{\lambda_1}}{I_{\lambda_2}} = \frac{(1 - e^{\frac{-7fL}{\lambda_1}})}{(1 - e^{\frac{-7fL}{\lambda_2}})} \frac{\lambda_2^5}{\lambda_1^5} \frac{e^{\frac{C_2}{T\lambda_2}}}{e^{\frac{C_2}{T\lambda_1}}} \\
&\frac{7fL}{\lambda} >> 1 && \frac{I_{\lambda_1}}{I_{\lambda_2}} = \frac{\lambda_2^5}{\lambda_1^5} \frac{e^{\frac{C_2}{T\lambda_2}}}{e^{\frac{C_2}{T\lambda_1}}}
\end{aligned} \tag{6}$$

The ratio $I_{\lambda_1}/I_{\lambda_2}$ is related to the emission measurements by Eq. (7)

$$\frac{I_{\lambda_1}}{I_{\lambda_2}} = \frac{10^{e_1}}{10^{e_2}} \tag{7}$$

where e is the emission measurement given on the vertical axis in Fig. 4. For λ_1 = 480 nm, Fig. 5 shows the calculated temperatures associated with various values of λ_2 for each limiting case. Data in this figure indicate that the uncertainty associated with these soot temperature estimates is on the order of $\pm$ 50 K. The values in Fig. 5 compare favorably with the calculated adiabatic flame temperature of 1576 K, especially for the limit $7fL/\lambda \gg 1$, which is reasonable since large amounts of soot were evident in the visualization experiments.

Figure 4 also compares emission spectra obtained from DNT decomposition to spectra obtained from a burning candle. The spectra are similar, supporting the idea that the DNT emissions are primarily from soot. The average temperature of radiating soot in the candle flame was also estimated with a two-wavelength pyrometry analysis. By assuming the ratio $7fL/\lambda$ is significantly less than unity or significantly greater than unity, the estimated temperatures of radiating soot particles varied from approximately 1429 to 1490 K for λ_1=480 nm and $450<\lambda_2<520$nm (using Eqs. 5 and 6). These values should approximately bound the average soot temperatures. The adiabatic flame temperature for combustion of heptane in air is listed[9] as 2290 K. The candle wax adiabatic flame temperature should be about the same, though

radiation losses from the candle may decrease the peak temperature slightly. The fact that the candle flame is a diffusion flame accounts for the large variation between the estimated soot temperature and the adiabatic flame temperature. This is because much of the soot in the candle flame will reside in cooler regions on the fuel side of the flame, away from the peak temperature zone. In the DNT bubbles, however, premixed flames will be present and soot will exist in high-temperature gas products formed after passage of the deflagration wave. These products may approach the adiabatic flame temperature, which is consistent with the present results.

Absorption Measurements

In addition to the emission spectra, absorption measurements were obtained while the samples decomposed in the molten salts. These measurements focused on detecting chemical species present in the salts. The energetic materials LX-04, LX-17, DNT, and the plastic binders Viton A and Kel-F 800 were each studied separately, and in each experiment spectra were collected at 50 to 100 ms intervals over the sample lifetimes in the molten salts. LX-04 and the plastic binders Kel-F 800 and Viton A were found to be very clean burning and did not absorb significantly at any wavelength investigated, indicating that the salt composition was not appreciably altered. In contrast, LX-17 and DNT showed significant absorption. Figure 6 shows representative absorption data for DNT for beam position 1 (see Fig. 2). For

DNT, an absorption peak centered at 276.5 nm appeared approximately 0.3 s after injection into the salts. This peak decreased in intensity until about 0.9 s after injection, after which it was no longer detectable. When the beam was positioned below the DNT sample (beam position 2 in Fig. 2), no absorption peaks were detected during DNT decomposition.

Technical DNT is a mixture of isomers, mainly 2,4- and 2,6-isomers.[10] The DNT analyzed in this study was purchased from Aldrich Chemical Co. (Milwaukee, WI). An analysis of the DNT samples used in this study, and the resulting spectrum, shown in Fig. 7, verifies that the DNT sample is mainly 2,6-DNT with a small amount of 2,4-DNT isomer. The two peaks in Fig. 7 at 230 and 250 nm correspond to 2,4-DNT and 2,6-DNT, respectively. As suggested below, the peak detected at 276.5 nm in the molten salt experiments is likely due to a para-nitrotoluene isomer, which would result from the decomposition of 2,4-DNT.

The chemical structure of DNT is similar to that of TNT. In an effort to analyze the chemistry associated with DNT decomposition, the assumption is made that at least initially, the thermal decomposition process of TNT is similar to that of DNT. Based on the literature,[11] the rate-determining step in the thermal decomposition of TNT may be either CH_3 oxidation or $C-NO_2$ homolysis reactions, depending on the temperature. In either case, an intermediate species present during each process is nitrotoluene. The most chemically stable form of nitrotoluene

occurs when the nitro group bonds to a carbon in the para-position (4-nitrotoluene).[12] Therefore, the decomposition rate of para-nitrotoluene will be slower than the other nitrotoluene isomers, and thus should be more likely detectable. Measurement of the spectra of para-nitrotoluene using our spectrometer under room temperature conditions and using methanol as a solvent indicates a peak wavelength corresponding to 274 nm. This absorbance peak has also been reported elsewhere.[13,14] Other isomers of nitrotoluene result in shorter peak absorbance wavelengths and do not correspond as well with spectra obtained during DNT decomposition.

Based on the above, the absorbance peak at 276.5 nm is most likely from para-nitrotoluene produced during the DNT decomposition process. The difference in absorbance peak wavelengths between para-nitrotoluene detected in methanol and in molten salt can be attributed to a difference in polarity of the solvents. An increase in solvent polarity can cause a shift in the wavelength of the peak spectra (the solvent effect).[15,16] The direction of the shift in peak wavelength, i.e., whether it is a red shift or a blue shift, depends on the interactions of the molecule with the solvent as well as the electrons that are involved with producing the spectra. For example, an increase in solvent polarity can cause a red shift for $\pi \rightarrow \pi^*$ transitions and a blue shift for $n \rightarrow \pi^*$ transitions. In the case of para-nitrotoluene, it is known that the peak wavelength shifts from

about 250 μm in the vapor phase to 285 μm in liquid water.[15] This red shift is caused by the polarity of the water. Because the molten salt eutectic (KCl-NaCl-LiCl) is an ionic liquid, the eutectic solvent should also promote a peak absorbance shift toward longer wavelengths. In this case, the shift observed is on the order of 2 nm (relative to a methanol solvent), and accounts for the difference in wavelength maxima between 4-NT in methanol and 4-NT detected during DNT decomposition in molten chloride salt. The stronger red shift noted above for water may be related to the fact that water has a much higher dielectric constant than either methanol or the chloride salts employed here.

Assuming para-nitrotoluene is the absorbing species in Fig. 6, the concentration of para-nitrotoluene can be estimated using Beer-Lambert's Law.[17]

$$A = a_m bc \tag{8}$$

In Eq. (8), the absorbance A is a measure of how much light is absorbed by a sample, a_m is the wavelength-dependent molar extinction coefficient, the path length b for each experiment is 2.0 cm, and c is the species concentration. The spectrometer software calculates absorbance using the following equation.

$$A = -\log_{10}\frac{(S-D)}{(R-D)} \tag{9}$$

In Eq. (9), S is the sample intensity, D is the dark intensity, and R is the reference intensity. The absorbance A is plotted in Fig. 6 on the vertical axis. For para-nitrotoluene concentration estimates, an a_m value of 11700 L/(mole cm) is used.[13] Using Eq. (8), para-nitrotoluene concentrations in the molten salt are estimated to vary from 4.8×10^{-5} mole/L, 0.2 s into sample decomposition and decreasing in intensity to 1.5×10^{-5} mole/L after 1 s. Because the concentrations calculated using Eqs. (8) and (9) are line-of-sight integral averages, actual peak concentrations could be higher. The overall lifetime of a 1 g DNT sample immersed in the 700 °C chloride eutectic is 1.7 s. Therefore, once the sample has completely decomposed, the peak attributed to para-nitrotoluene is no longer detectable and the salts are not chemically altered at the end of the DNT decomposition process.

When the beam is aligned below the sample (location 2), no absorbance is observed during DNT decomposition, i.e., the para-nitrotoluene detected above the sample is not apparent at this beam position. At beam location 1, however, para-nitrotoluene may be present in the gas bubbles that decompose and rise to the surface of the salt. As observed in the visualization experiments, bubbles are not produced below the sample (Fig. 3). In fact, the thin film circulates liquid flow away from the base of the cuvette and toward the top of the sample, where the bubbles are formed (liquid flows were visualized by observing

trajectories of small soot particles present in the bath). If para-nitrotoluene is formed during decomposition, this decomposition process might occur within the bubbles. Because the bubbles do not intersect the beam when it is positioned below the sample, it is reasonable to expect that para-nitrotoluene would not be detectable in this location. An alternative explanation is that the para-nitrotoluene detected above a DNT sample was present in the liquid. By the time the liquid has been transported to a position underneath the sample, the para-nitrotoluene may have reacted. The presence of the solvent shift, however, which would apply to para-nitrotoluene in the liquid but not the gas, indicates that the para-nitrotoluene that was detected was actually in the liquid salts.

Regarding LX-17, data show that species in the salt bath varied with time as well as with position in the bath. Figure 8 shows representative time series data for LX-17 absorbance at beam position 1. An absorption peak is first observed approximately 6 s after sample injection into the molten chloride salts. The peaks shift in wavelength (between 295 and 315 nm) and vary in intensity over time for about 13 s, after which the absorption peaks disappear slowly and are no longer detectable. Because 0.3 g samples of LX-17 have a lifetime of about 22 s in 700 °C molten chloride salts, the absorption peaks are an indication of the presence of intermediate chemical species. Several distinct species may be absorbing in this region, including CH_2O, CHO, CN^*, CH, OH, O_2, O_3, and NH.[18] For example,

formaldehyde vapour absorption is complex and not readily identified except by comparison of spectrograms; strong bands occur at 293.1, 303.6, and 314 nm.[19] Other species such as CHO also exhibit bands at 301 and 311 nm, and OH bands occur at 302, 306, and 307 nm.[18] In contrast to the DNT results discussed earlier, the transient shifts in LX-17 peak wavelengths indicate that varied chemical species were present in the bath as time progressed. These species temporarily altered the chemistry of the molten salt bath, but over time additional chemical reactions eliminated the existence of these peaks, indicating that the chemistry of the molten salts returned to its original state.

When LX-17 decomposes and the beam is positioned below the sample, different spectral peaks are detected. Figure 9 shows time series data for LX-17 absorbance in the molten chloride eutectic. After about 5 s into the sample decomposition history, strong absorbance between about 526 and 590 nm was measured for a duration of about 1 s. Because of the effects of solvent shifts, it is difficult to identify the species responsible for these spectra. It is also possible that more than one species may have been responsible for these spectra, which also makes interpretation difficult. One species that may have been present, however, is NH_2, which has been suggested as being an intermediary that is produced relatively early in the decomposition history of TATB.[20,21] Apparent α bands for NH_2 (maxima) have been reported in the range 526.5 - 665.2 nm, the strongest being at 571.3 nm.[22] In addition, the strongest features in NH_2 absorption (reported at

570.8 nm) tend to degrade to the violet.[18] The relative ratios of the absorbance at 571 nm to those at 540 and 600 nm in Fig. 9 do not appear to follow this behavior. This may be due to spectrometer limitations approaching 600 nm (i.e., spectrometer roll-off). As a result, absorption in this range does suggest the presence of an intermediate chemical species that may correspond to NH_2.

It is also noted that these spectral data for NH_2 are from gas-phase measurements where solvent effects would not have been present. It is not clear how the molten salt bath used here would affect the spectra of NH_2. It has been stated, however, that solvent shifts can be small when NH_2 groups are added to benzene.[15] If this is also the case for the NH_2 radical, then the gas-phase data support the idea that NH_2 may have been present.

Another possible contributor to the peak spectra appearing in the range 526 and 590 nm is NO, which is a known product of TATB decomposition and which also absorbs strongly at about 600 nm in the gas phase.[18] If NO was present in the molten salt, a blue shift in the range of 15 nm in the peak absorbance spectra would be needed to produce the experimental data that have been obtained. A solvent shift of this magnitude is not unreasonable, and as a result we cannot rule out the possibility of NO.

At later times, after 14 s into sample decomposition, additional species absorb between 330 and 370 nm. This absorbance continues for approximately 6 s and fully diminishes at 22 s into

sample decomposition, i.e., when the sample is almost fully decomposed. Species absorbing in this wavelength region (and which are potentially relevant to these studies) include CH_2O, C_2, OH, CO, CHO, HCl^+, CO_2, ClO_2, OH^+, NO, CN, CO^+, NH, CH, and HNO_2, with the most strongly absorbing being HNO_2.[18] In fact, gas-phase HNO_2 absorbance spectra[18] correspond very well with the spectra observed here. The gas-phase HNO_2 spectra display a maximum at 354 nm and a full-width half-maximum bandwidth of 30 nm, which corresponds very well with the data obtained in this study and shown in Fig. 9. Again, however, it is noted that the effects of a chloride-bath solvent shift on HNO_2 spectra are not characterized. It is also worth mentioning that the NO_2^- ion dissolved in potassium nitrate molten salt displays an absorbance peak at about 359 nm,[23] which is within the range of the data considered here. NO_2 is known to be a decomposition product of TATB, and formation of the NO_2^- ion in the melt could contribute to these spectra as well.

Other researchers[24] have also studied the condensed phase thermal decomposition of TATB and found that the major decomposition products formed are the lower molecular weight species H_2O, HCN, CO, HNCO, CO_2 and C_2N_2. Many of these species are consistent with the spectra observed in this study. However, this is the first time the possible presence of HNO_2 has been reported.

It is noted that the delays associated with appearance of the initial absorbance peaks are consistent with earlier data on

gas evolution behaviors of LX-17 and DNT in molten salts. In previous studies,[3,4] it was shown that there is an induction (heatup) period after injection during which gas evolution rates are low. Following this induction period, gas evolution rates were observed to become very vigorous. For DNT, the induction period was typically of the order of a few hundred ms in chloride salt baths,[3] while for LX-17 in chloride salt baths the induction period was on the order of about five s.[4] Based on these results, delays in appearances of the initial absorbance peaks likely occurred because initial reaction rates were small, and measurable amounts of species appeared after the induction periods were over and reaction rates became larger.

Recounting the qualitative behavior of LX-17 decomposition in molten salt helps to explain further the time dependencies of the observed spectra. When LX-17 is immersed in the molten salt, heating (and subsequent decomposition) begins from the outside of the sample inward. During LX-17 decomposition in molten chlorides, a carbon residue with approximately the same dimensions as the original LX-17 sample is produced.[4] Laser desorption time of flight mass spectrometry indicates that this residue is a result of TATB decomposition and not Kel-F 800 binder decomposition.[4] Based on all of this information, we offer the following scenario for the time history of decomposition of an LX-17 sample. During the early stages of decomposition, the binder, which produces decomposition products that do not absorb in the UV-VIS wavelength regime, likely decomposes during the

initial heatup period of a sample. After about 5 s, the TATB begins decomposing as well, producing an early-time spectral signature for a brief time period. This spectral signature may correspond to species that appear early in the decomposition history of TATB, such as NH_2. Following this, further decomposition products such as CH_2O, CO, or CO_2 may be detected.

The possible early appearance of NH_2 is consistent with observations of the decomposition kinetics of TATB. For example, it has been suggested that a deamination reaction that produces NH_2 is the primary step in the decomposition of TATB,[21] and other researchers have indicated that NH_2 is an important species in the early decomposition history of TATB.[20] The early-time signature detected in these experiments may result from NH_2 (or another species that appears early in the decomposition history) produced near the outside edges of the samples. As the samples decompose, the porous carbon matrix form from the edge of the sample inward, and any species produced in the sample interior would have to pass through the matrix before entering the liquid. These species would have additional time to react as they passed through the matrix, which would be quite hot from exposure to the molten salts. As a result, species leaving the sample at later times may be different than the initially detected species. This explains why the overall absorption spectra varied with time.

Finally, it is worth noting that LX-17 decomposition does not generate the same circulation patterns observed with DNT.

During LX-17 decomposition, bubbles formed at the top, base and sides of the samples. The resulting molten salt flow (as observed by following soot particle trajectories) circulated away from the bottom of the sample and toward the base of the cuvette in the opposite direction as observed during DNT decomposition.

CONCLUSIONS

The absorption measurements indicate that for the wavelengths investigated, intermediate chemical species can be present in the salts and that species can vary temporally as well as with location relative to the samples. Emission measurements show that DNT emits radiation strongly in the visible region, while LX-17 and LX-04 emit radiation weakly in this wavelength region. This result can be explained by understanding the physical decomposition processes. Because the bubbles generated from DNT decomposition grow in size and darken in color, chemical reactions occur in the gas phase. These reactions result in an abundance of soot. At the high gas-phase temperatures that were present, soot emits light vigorously in the visible spectrum.

It is also noted that once samples had completely decomposed, no absorption was detected in the molten salt baths for any of the energetic materials investigated. This result suggests that the salt composition was not appreciably altered after the destruction processes. In practice, it would be advantageous to re-use the molten salts because of the difficulties associated with cleaning and replacing the eutectic.

Because the bath does not appear to be chemically altered after the destruction process, it seems reasonable to conclude that the eutectic may be used repeatably, with virtually no loss in sample destruction efficiency, and with only periodic purging.

ACKNOWLEDGEMENTS

The financial support of the Energetic Materials Center at Lawrence Livermore National Laboratory (LLNL) is gratefully acknowledged. Thanks are also due Dr. B. Watkins (LLNL) and Prof. P. Kelly (UC Davis) for helpful discussions.

REFERENCES

1. R. S. Upadhye, B. E. Watkins, C. O. Pruneda and W. A. Brummond, *Molten Salt Destruction as an Alternative to Open Burning of Energetic Material Wastes*, Report UCRL-JC-117252, Lawrence Livermore National Laboratory, Livermore, CA (1994).

2. J. Li and P. K. Dasgupta, *A Simple Instrument for Ultraviolet-Visible Absorption Spectroscopy in High-Temperature Molten Salt Media*, Rev. Sci. Inst. 71, 2283 (2000).

3. M. B. Lacchia and B. D. Shaw, *Studies of Energetic and Nonenergetic Materials Immersed in Molten Salts*, Combust. Sci. Tech. 139, 59 (1998).

4. M. L. Pantoya, B. D. Shaw and E. A. Megas, *High Speed Imaging of LX-04 and LX-17 Decomposition in Molten Salts*, Prop., Expl., Pyrotech. 25, 19 (2000).

5. A. Citarella, *Optical Access to Molten Salt Destruction of High Explosives*, Master of Science Thesis, University of California, Davis (1996).

6. W. C. Reynolds, *The Element Potential for Chemical Equilibrium Analysis: Implementation in the Interactive Program STANJAN*, Department of Mechanical Engineering, Stanford University (1986).

7. R. Siegel and J. R. Howell, Thermal Radiation Heat Transfer, 3rd Ed., Hemisphere Publishing Co., Washington DC, (1992).

8. I. M. Kennedy, W. Kollmann and O. Schafer, *Modeling of Radiation from Luminous Turbulent Diffusion Flames*, Proceedings of the 35th Aerospace Sciences Meeting, AIAA paper no. 97-0252, Reno, NV, January (1997).

9. I. Glassman, Combustion, Academic Press, San Francisco, (1977).

10. J. Yinon and S. Zitrin, The Analysis of Explosives, Pergamon Press, New York (1981).

11. T. B. Brill and K. J. James, *Decomposition of Energetic Materials. 62. Reconciliation of the Kinetics and*

Mechanisms of TNT on the Time Scale from Microseconds to Hours, J. Phys. Chem. 97, 8759 (1993).

12. J. March, Advanced Organic Chemistry: Reactions, Mechanisms and Structure, McGraw-Hill Publishing Co., New York, (1977).

13. Sadtler Research Laboratories, Sadtler Ultra Violet Spectra, p. 1293 UV, Philadelphia, PA (1966).

14. C. P. Conduit, *Ultraviolet and Infrared Spectra of Some Aromatic Nitrocompounds*, J. Chem. Soc. 665, 3273 (1959).

15. H. H. Jaffe and M. Orchin, Theory and Applications of Ultraviolet Spectroscopy, Wiley, New York (1962).

16. A. Knowles and C. Burgess, Practical Absorption Spectrometry, Chapman and Hall Publishing, New York, (1984).

17. G. H. Schenk, Absorption of Light and Ultraviolet Radiation: Fluorescence and Phosphorescence Emission, Allyn and Bacon, Inc., Boston, (1973).

18. R. Pearse and A. Gaydon, The Identification of Molecular Spectra, John Wiley and Sons Inc., New York, (1963).

19. V. Henri and S. A. Schou, Zeit. fur Phys. 49, 774 (1928).

20. M. Farber and R. Srivastava, *Thermal Decomposition of 1,3,5-Tramino-2,4,6-Trinitrobenzene*, Combust. Flame 42, 165 (1981).

21. P. S. Makashir and E. M. Kurian, *Spectroscopic and Thermal Studies on the Decomposition of 1,3,5-Triamino-2,4,6-Trinitrobenzene (TATB)*, J. Therm. Analysis 46, 225 (1996).

22. A. Fowler and J. S. Badami, *The Spectrum of the Hydrogen-Nitrous Oxide Flame*, Proc. Royal Soc. A 133, 325 (1931).

23. P. D. Smith, "Electronic Absorption Spectra of Molten Salts," in Molten Salt Chemistry, M. Blander, ed., Interscience Publishers, New York, 1964 p. 427.

24. R. Behrens, T. A. Land, W. J. Siekhaus, and M. F. Foltz, *Condensed-Phase Thermal Decomposition of TATB Investigated by Atomic Force Microscopy and Simultaneous Thermogravimetric Modulated Beam Mass Spectrometry (STMBMS)*, 10th International Detonation Symposium, Boston, MA, ONR 33395-12, 181 (1993).

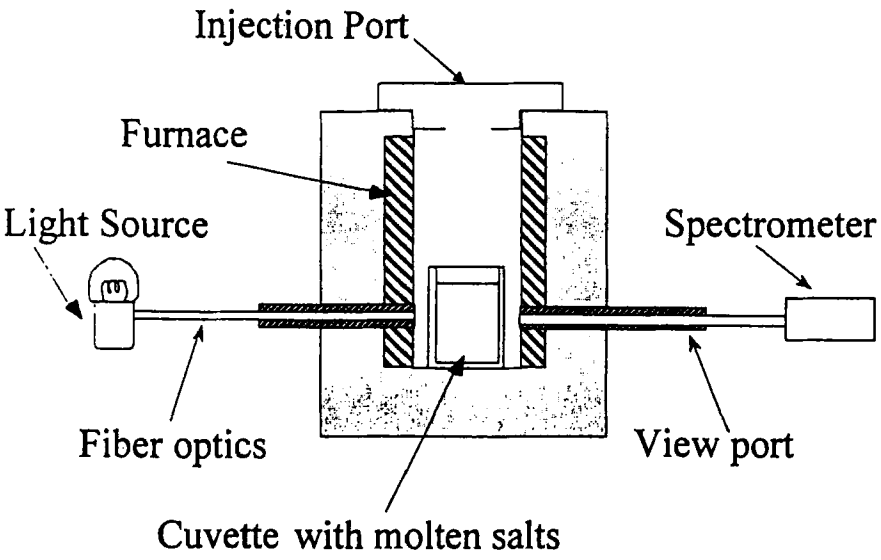

FIGURE 1

Experimental setup for the spectroscopy experiments.

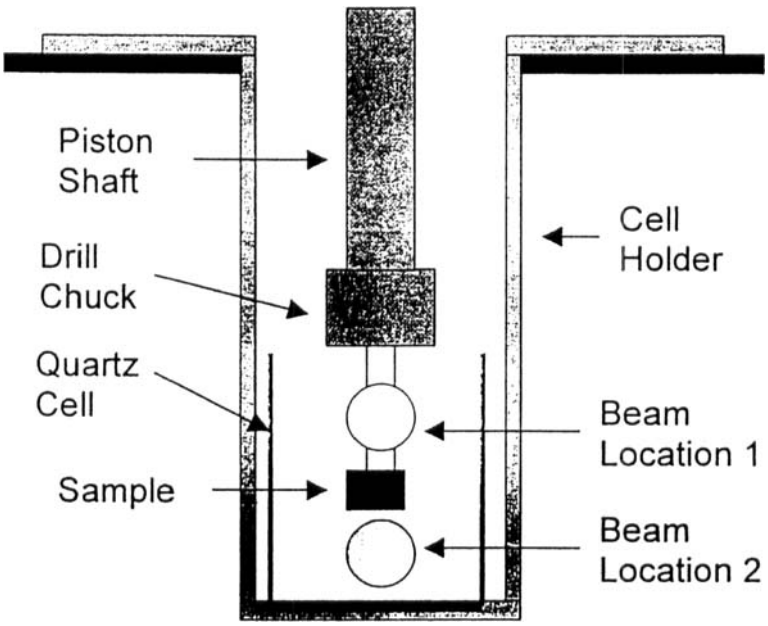

FIGURE 2

Schematic showing the sample locations and beam positions.

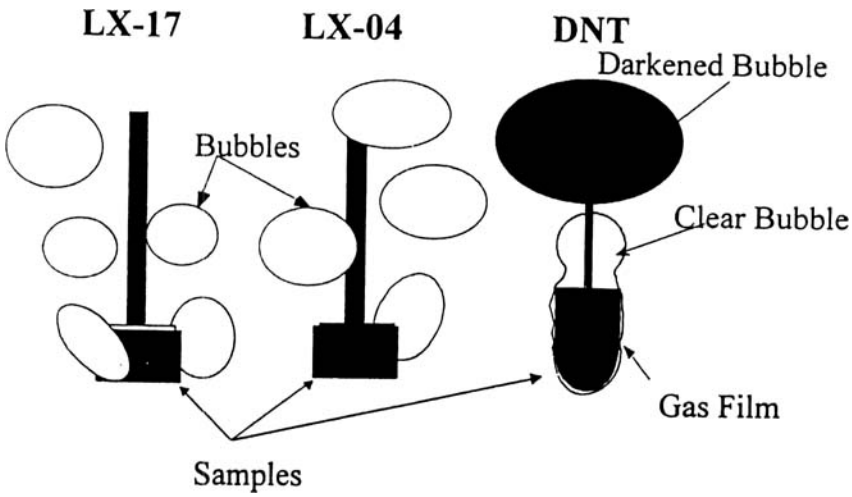

FIGURE 3

Schematic of LX-04, LX-17, and DNT decomposition behaviors.

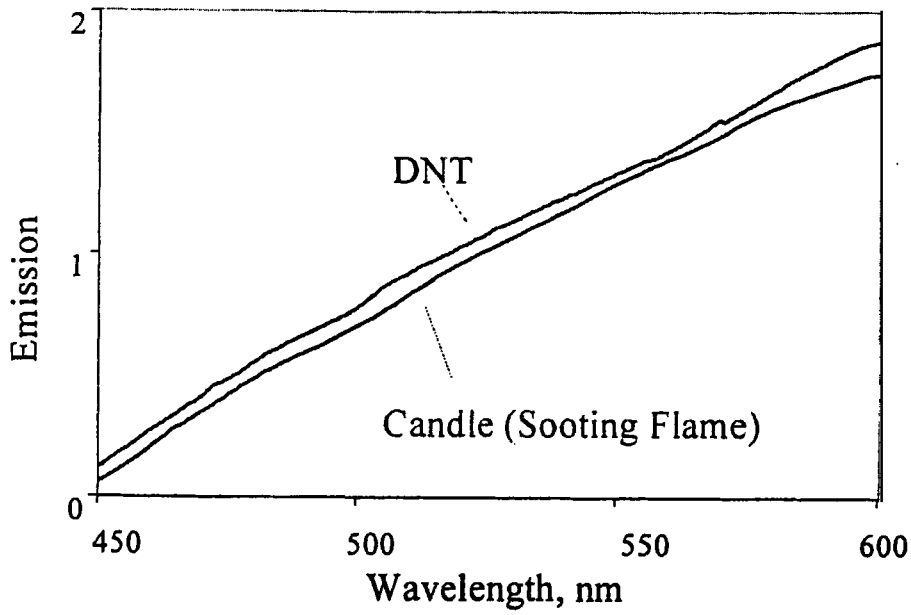

FIGURE 4

Emission from a wax candle flame and from DNT decomposition. The vertical axis is $\log_{10}$ of the emission.

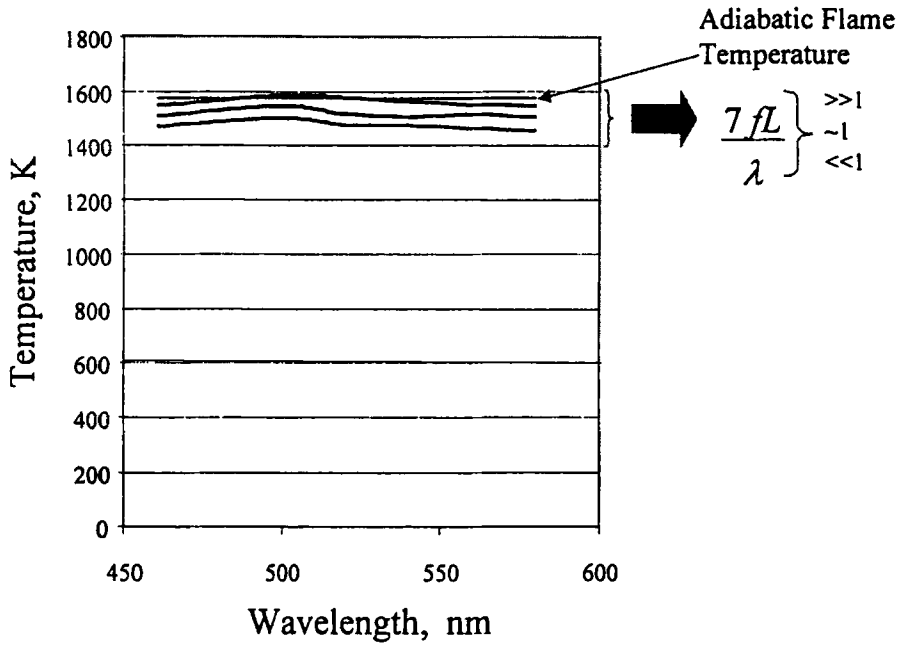

FIGURE 5

DNT soot temperatures estimated using Eq. (6) (λ_1 = 480 nm).

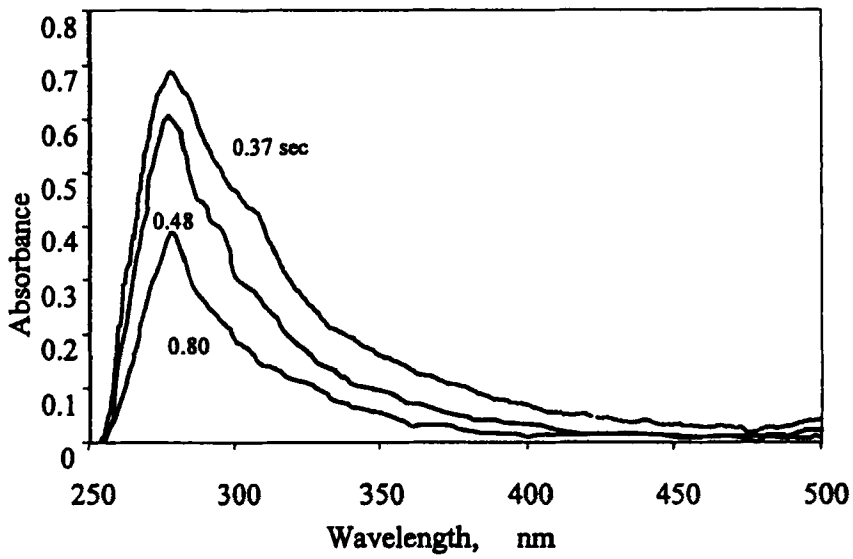

FIGURE 6

Transient absorbance (beam location 1) during DNT decomposition. The vertical axis is $\log_{10}$ of the absorption.

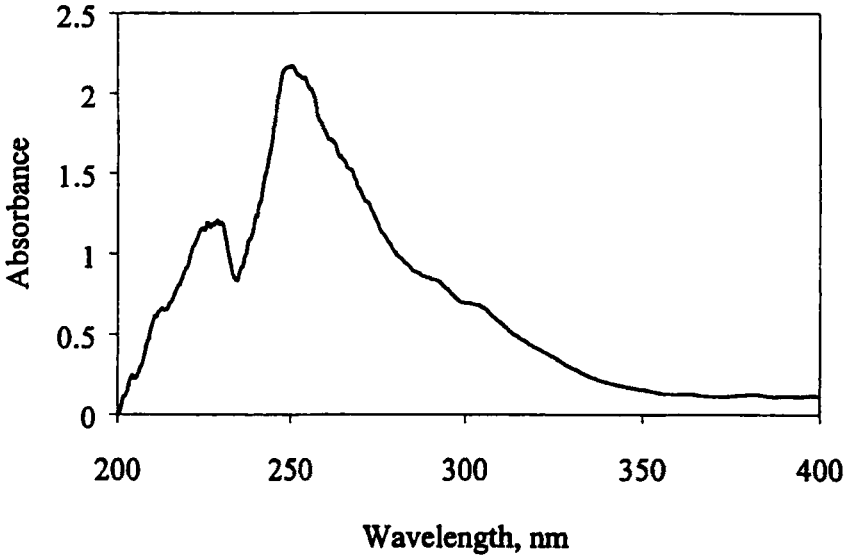

FIGURE 7

DNT absorbance spectrum in methanol. The peaks at about 230 and 250 nm correspond to 2,4-DNT and 2,6-DNT, respectively.

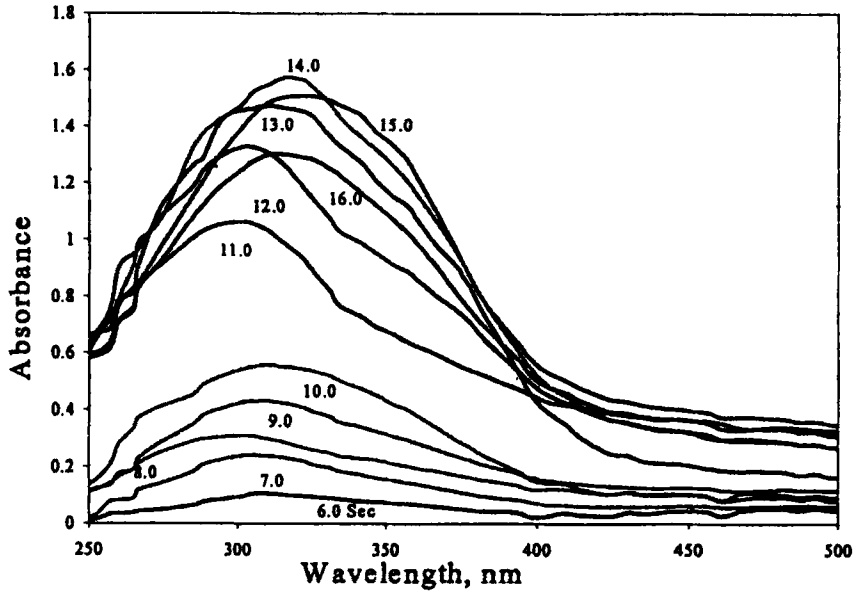

FIGURE 8

Time series absorbance spectra (beam location 1) obtained during LX-17 decomposition. The first peak was detected 6.0 s after injection.

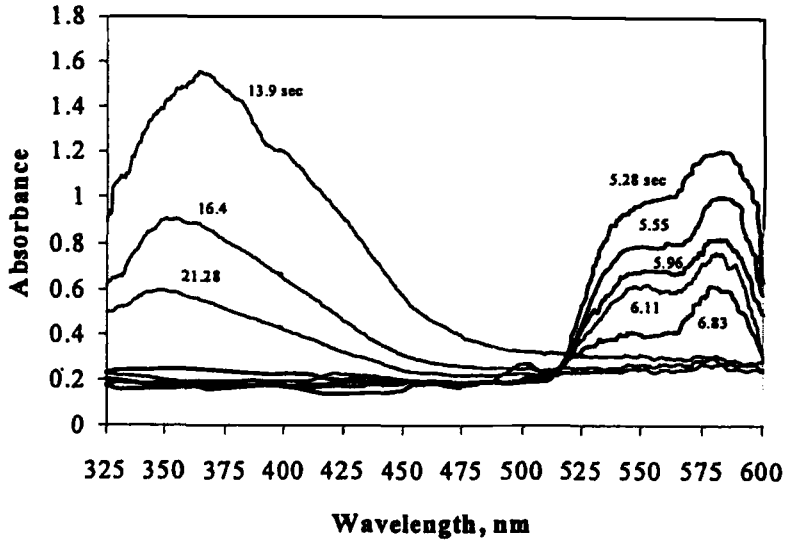

FIGURE 9

LX-17 absorbance (beam location 2). Absorbance over the wavelength range 525-600 nm was detected from 5.28 s to 6.83 s after injection, while absorbance over the wavelength range 330-375 nm was detected from 13.9 s to 21.28 s after injection.